DEVELOPMENT OF NATIONAL MRO CAPABILITY FOR A BASIC TRAINER AIRCRAFT: FLIGHT AND GROUND TESTS

Tuomas Korteniemi[1*], Jouni Pirtola[1], Antero Miettinen[1], Sauli Liukkonen[2], Aslak Siljander[2], Olli Orell[1,3], Jarno Jokinen[3], Mikko Kanerva[3]

[1] Patria Aviation Oy (Patria), Lentokonetehtaantie 3, 35600 Halli, Finland
[2] Technical Research Centre of Finland Ltd (VTT), Kemistintie 3, 02044 Espoo, Finland
[3] Tampere University (TAU), Korkeakoulunkatu 6, 33720 Tampere, Finland

Abstract: Patria has an ongoing program to develop a partial national maintenance, repair and overhaul (MRO) capability for the new basic trainer aircraft of the Finnish Air Force (FINAF). The capability is developed since no original design data is available. This paper presents the research performed on the flight tests and static ground tests of individual components as two subprojects of the MRO capability program.

The flight test subproject included instrumentation of the test aircraft, ground calibrations, flight tests and analysis of results. The instrumentation suite included strain gauges, temperature sensors and various flight parameter sensors. The instrumentation suite was ground calibrated to enable calculation of global load components. Flight test results have already been utilized when designing repairs and modifications for the aircraft.

For the ground tests, the instrumentation of the aircraft components was extended to include more strain gauges and also displacement sensors. In addition, full-field deformation data was captured simultaneously using digital image correlation (DIC). During the ground tests, all major components of the aircraft were individually tested. In this paper, tests of L/H main landing gear leg and L/H wing are discussed in more detail. Results obtained with different techniques are compared to assess the applicability of DIC.

Keywords: Flight testing, ground testing, reverse engineering, MRO, basic trainer aircraft

INTRODUCTION

It has been in the culture of the FINAF to be self-sustaining to a certain level with their aircraft. This makes domestic life cycle support, modifications and repairs possible. With this background the Finnish Defense Forces (FDF) has funded a program in which Patria with its partners build a basic technical understanding of the Grob G115E and develop a partial national MRO capability for the new basic trainer focusing on the airframe and some of its main components like the landing gear and the engine mount. Because the design data of the aircraft is not available, the data package has to be reverse engineered or built up from different sources.

Grob G115E airframe is a composite structure, so it was obvious from the beginning that a complete data package will not be possible in practice because of unknown composite lay-ups in several locations. Thus, the selected approach was to collect as much data as practical during the program and supplement the data package in the future when additional information comes available e.g. because of damages during operation.

The first step of the program was an aerodynamic model of the aircraft and initial computations with it [1]. Applications and enhancements to the CFD model were made few years later [2]. Loads affecting on the aircraft were also estimated using the simplified methods provided by FAR23 regulations [3].

The next steps of the national MRO capability program included two subprojects: A flight test program and a ground test program of individual components, which are described in this paper.

FLIGHT TESTS

Flight test program

The aim of the flight test subproject was to gain insight on the structural behavior of the aircraft by gathering in-flight structural response data (strains) from selected components of the aircraft and to determine the flight mechanic characteristics of the aircraft. The flight test project was a so called mini-OLM i.e., a relatively small-scale operational load measurement project carried out in co-operation between Patria, FINAF and VTT.

In total the flight test program consisted of 22 flights and 21 flight hours. Each flight contained dedicated test points and flight maneuvers to cover essential FINAF's flight training syllabi and designed flight envelope to define limit loads. The flight test program consisted of 17 test points to cover loads from taxying, take offs and landings, 23 test points to cover the flight envelope and 49 test points to cover FINAF's flight training syllabi. Since many of the test points were flown with varying center of gravity and mass, altogether 152 test points were recorded. [4, 5]

Flight test instrumentation

For the mini-OLM project, a total of 40 resistance strain gauge channels were instrumented on the test aircraft for measuring in-flight strains. In addition to the strain gauges, sensors measuring the temperatures of the structures were installed at 8 different locations. Additional captured in-flight parameters included airspeed, altitude and normal acceleration next to center of gravity. The overview of the flight test strain gauge instrumentation is given in table 1.

Table 1: The overview of the strain gauge instrumentation.

Component	*Normal Strain*	*Shear Strain*	*Bending Strain*
Wings	-	8	9
Fuselage	-	6	2
Vertical stabilizer	-	1	2
Horizontal stabilizer	-	-	2
Control surface rods	6	-	-
Engine mount	4	-	-

All strain gauge channels were implemented as Wheatstone full-bridge type set-ups, with four active arms on each. Full-bridge configurations were used to maximize the stability of the signals and to minimize the temperature effects on the measured strain values. The used full-bridge strain channels measured normal-, shear- and bending strains mainly from composite structures but also including steel and aluminum components.

Acra KAM 500 Data Acquisition Unit (DAU) was used to record the strain gauge signals both in the mechanical ground calibrations as well as in the subsequent actual flight tests. All strain gauge data were

recorded in the flight tests using simultaneous sampling with 320 Hz antialias-filtering and 1280 Hz sample rate per channel. Similar DAU setups were applied on the ground calibrations except the sample rate (10 Hz). The flight parameters airspeed, altitude, normal acceleration and temperatures were recorded with the same DAU but using 10 Hz filtering and 40 Hz sample rate.

In addition, a separate inhouse-made DAU was used to collect flight mechanic data to support future load case generation. Measured parameters included for instance GPS location, airspeed, altitude, attitude, linear accelerations along all three axes, and angular velocities around all three axes. The sample rate of this inhouse-made DAU depended on the recorded quantity, linear accelerations and angular velocities being recorded with the highest sample rate. [6]

Mechanical Ground Calibrations

Mechanical ground calibrations were performed in two phases (off-aircraft and on-aircraft). In the first phase, the strain gauge instrumented control rods of the ailerons, flaps, rudder and elevator were mechanically calibrated off-aircraft to get the relationship between the measured strain and normal forces acting on these.

In the second phase, once the strain gauge instrumented aircraft was re-assembled into an airworthy configuration, a series of on-aircraft ground calibrations were performed. The aim of the ground calibrations was to get an understanding of the strain gauge signal responses under external clearly defined loading and support conditions. Calibrations were conducted for wing, fuselage, stabilizers, and engine mount separately. In addition, after being installed back to the aircraft, the control rod strains were also calibrated in various position angles of the control surfaces, with respect to the control surface hinge moment. Figure 1 provides an overview of the on-aircraft calibrations. Altogether 62 calibration load cases were recorded for the assembled aircraft.

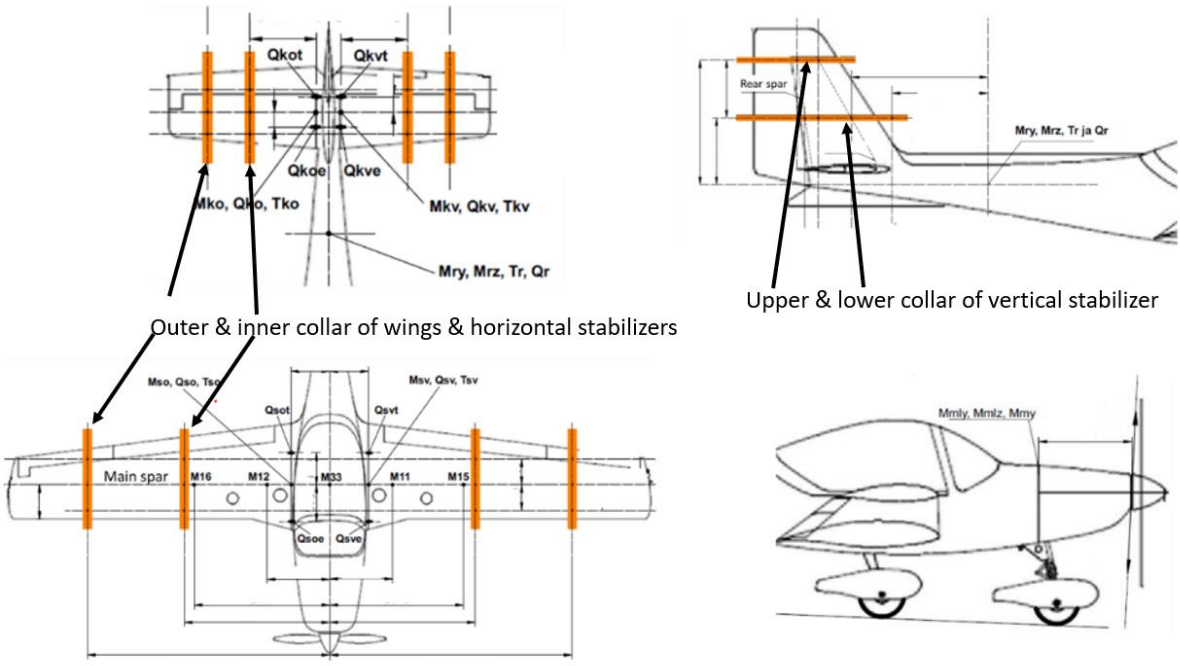

Figure 1: An overview of the on-aircraft ground calibrations. External vectorial loads applied via collars on each component.

Based on the ground calibrations, influence coefficient matrices were constructed for each component, describing the relationship between the measured strains and the external force magnitudes acting on them. The matrices were defined using each load level of each calibration case as an input data step and defining a linear neural network solution minimizing the error with least squares method. In linear case, the neural network becomes a single layer system consisting of matrix of influence coefficients *W* and

a zero-condition vector *b*, describing the relationship of the measured strains ε and applied external loads *F*, see Equation 1.

$$\{F\} = [W]\{\varepsilon\} + \{b\} \tag{1}$$

For the wing, calibrations were performed in two configurations: aircraft standing on ground, weight on wheels and aircraft jacked up on supports. The wing influence coefficient matrix was constructed using the latter configuration as this better describes the loading and responses during the flight.

Figure 2 shows the L/H wing vertical shear force Q_{sv} and wing root bending moment M_{sv} correlation in the wing mechanical calibration cases. Each marker represents one load step used in the input data set. In the figure, horizontal axis shows the applied loads and vertical axis the calculated values. In the performed calibration cases, the correlation between the measured and the calculated load values can be seen in figure 2. For the wing, altogether 15 load components were calculated from the strains, including 7 bending moments, 6 shear forces and 2 wing torsion moments. Similar approach was used for the other components yielding altogether 52 virtual calculated channels.

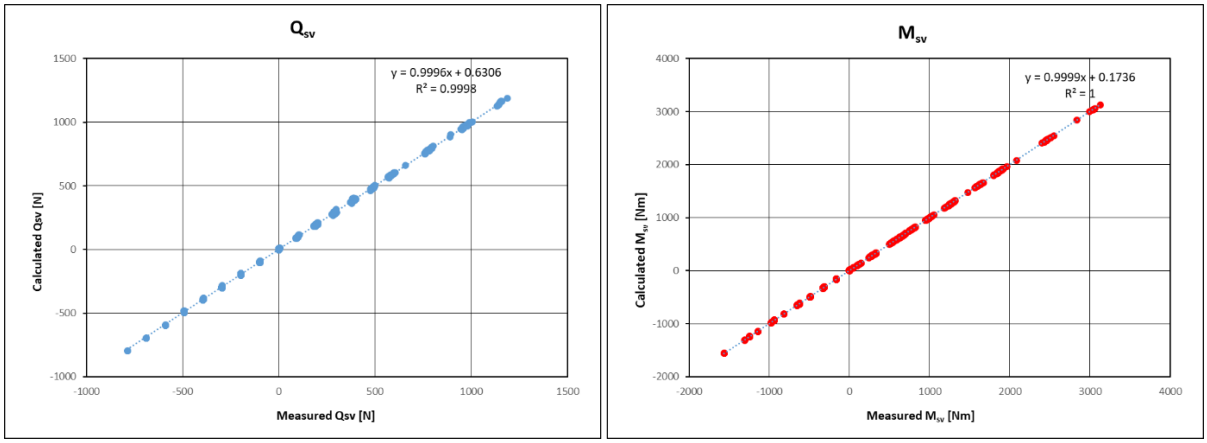

Figure 2: L/H wing vertical shear force Q_{sv} and wing root bending moment M_{sv} correlation in the wing mechanical calibration cases. Horizontal axis - measured, Vertical axis - calculated.

Analysis of flight tests

After the completion of flight tests, all recorded flight data were evaluated using various data integrity checks, including minimum and maximum value detection, as well as plotting signal time histories for all measured channels. Strain data were then processed using the influence coefficient matrices defined with the ground calibration data for the different structural components. This yielded first preliminary values for the virtual load component channels.

In the next analysis phase, all 152 test points were searched and isolated from the flight data. The flight crew determined the on-condition points, where the test point and hand-written supplementary test data such as control force measurements were in best alignment. All these test points were then analyzed defining minimum and maximum values for each, as well as plotting each isolated maneuver in a zoomed time scale. Both measured strains, as well as calculated virtual channels, were analyzed with a similar approach. Figure 3 shows an example of the L/H wing root shear force Q_{sv} and bending moment M_{sv} virtual load channels together with normal acceleration (NACg) from one flight test time zoom.

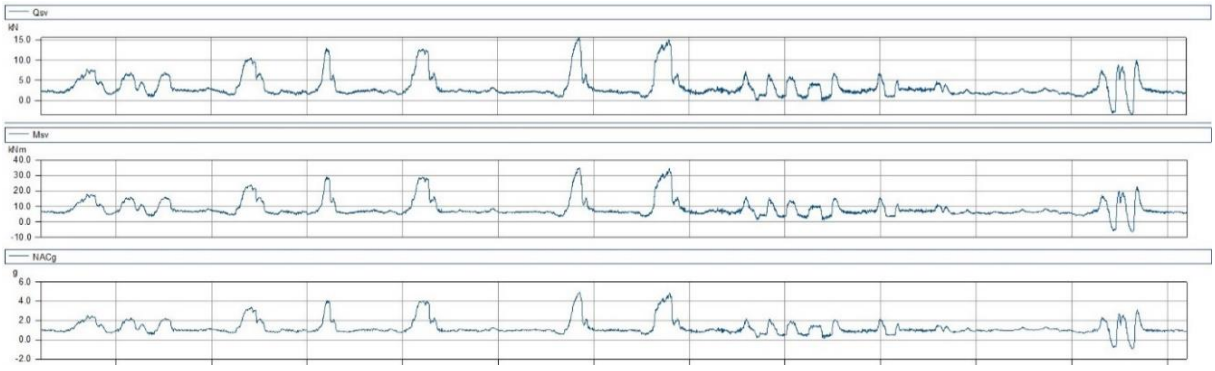

Figure 3: L/H wing vertical shear force Q_{sv}, wing root bending moment M_{sv} and normal acceleration NACg from a flight test.

The load signals calculated from the measured strains are based on the performed mechanical ground calibrations. It should be noted that, for practical reasons, the load and strain levels in the performed mechanical ground calibrations were small in magnitude compared to the actual in-flight loads and strains. Thus, the calculated loads given by the influence coefficient matrices with in-flight data should be viewed critically, as they are strongly extrapolated. The deeper scrutiny of these calculated values is future work to be done when this data is used in the MRO activities.

Flight test results

During the flight test project, the largest measured strains were found in the wing. From the wing surfaces, bending strains of magnitude +1700 / -700 μm/m during 6g windup turn and -3g steady state push down (SSPD) were recorded. The tensor shear strains in the wing surfaces were of magnitude ±500 μm/m during -3g SSPD and 6g abrupt pull-up. Largest bending strains in the wing main spar composite flanges were of magnitude +1000/-500 μm/m during 6g windup turn and -3g negative loop or -3g SSPD. Bending strains of similar magnitude were also encountered in the steel plates of the wing middle joint during same maneuvers. The material data of the composite structures is yet to be determined but based on the ultimate strains given in the available standards, the flight test data suggests that the composite structure has some fail-safe factors included in its design.

Calculated global load components of the wing were of magnitude +20/-10 kN for wing shear force and +40/-20 kNm for wing bending moment during 6 g windup turns and -3g steady state push downs. The largest measured hinge moments were of magnitude 200 Nm for flaps during steady heading side slips (flaps fully extended). All results, including description of the aircraft instrumentation and calibrations are reported in the reference [5].

The flight test results, especially the hinge moments and wing strains have already been utilized when analyzing the issues regarding hinge bracket attachments. The flight test results have also enabled the analysis of wing surfaces when designing access holes to the wing surfaces when carrying out repairs inside the wing. Flight tests also showed that the strains in the structure are insensitive to ambient temperature.

GROUND TESTS

Ground test program

The ground tests were aimed to provide measured strain and displacement data from the components under known loadings and support conditions for adjusting and validating the future FE-models of the components. The tested components were L/H wing, fuselage, horizontal stabilizer, aileron, flap, rudder, both elevators, engine mount and L/H main landing gear leg. The test program was conducted in co-operation between Patria, VTT and TAU.

During the ground tests, structural responses were measured from each component when loaded using a clearly defined load and support conditions. For these tests the instrumentation was extended to multiple displacement sensors and large number of strain gauges. The load levels were kept low since the test aircraft will return to FINAF service. 3-D Digital Image Correlation (DIC) method was utilized as an additional measurement technique in large part of the measurements to get full-field deformation data from the tested components. DIC was selected to be an additional measurement technique since it had not been earlier utilized in the Finnish aviation industry to components of this size. Therefore, the tests also provided information about its applicability for later projects.

Depending on the component, up to 35 load cases were used. The entire program consisted of 201 load cases and DIC was utilized in 113 of these. In all load cases, the overall load was applied in multiple discrete load steps to monitor the linearity of the response.

Support conditions and load levels

For most of the components the support conditions in the tests corresponded well to those as installed in the aircraft. The main landing gear leg was attached to the test jig using original attachment brackets and bolts. Horizontal stabilizers were attached together using original bolts and the stabilizers were supported by the four stabilizer root shear pins attached into holes in the test jig. Wing had a symmetric load case support at wing main spar root (free translations in aircraft symmetry plane and spar twist rotation - other movement/rotations and warping restrained) with spar axial load and bending moments measured and vertical supports with load sensors under the wing root shear pins. Wing support conditions are shown in figure 4. Fuselage was supported on 3-axis load sensors at each of the four wing root shear pin bearings.

Figure 4: Wing support showing also the wing upper surface DIC pattern.

The attachment of the engine mount to test jig corresponded to that in aircraft fuselage firewall, but for clarity of boundary conditions when comparing with FE-model, an engine dummy was attached to the engine mount without the rubber bushings between them. For the same reason the control surfaces having 3-5 hinges were supported only at two (three for the long flap) hinge locations to achieve clear and isostatic support conditions.

Depending on the correspondence of loads introduction and support conditions in tests to those in the aircraft, the applied load and estimated support reaction load levels in tests were restricted to 25%...50% of the load values calculated according to FAR23 and/or from the flight test measurements. In addition, applied overall load levels were limited by the local loading effects due to the usage of relatively narrow loading collars. Since only limited load levels were applied it was clear that only stiffness data will be available from the ground tests.

Ground test instrumentation

For the ground tests the instrumentation suite was expanded with additional strain gauges. In this instrumentation, most of the original strain gauges used in the flight tests were utilized, either as is or in many cases by isolating one or more arms from the original full bridge configuration as a new independent measuring channel. In addition, 227 new strain gauge channels were installed, consisting of 131 single arm quarter bridges for normal strains and 66 two arm half bridges for shear strains. Also

strain gauge rosettes were used in some cases to detect three strain components, 30 channels total. The ambient temperature was constant during load cases, which ensured that thermal strains were excluded from the measurement results. All quarter bridge strains were measured using three-wire connections.

In addition to the above expanded strain gauging, displacements of the components were measured using laser distance sensors with varying ranges from 10 mm to 100 mm. Table 2 shows the overview of the aircraft component strain gauge and displacement sensor set up. Maximum of 8 displacements points were measured simultaneously in any load case. For example, the fuselage was loaded with four different configurations, with different displacement set ups on each, resulting altogether 28 displacement measurement points.

All loads applied to the components were measured with load cells, varying from one to four loads at the same time. All data was captured within the DAU using simultaneous sampling with 10 Hz sampling rate.

Table 2: The overview of the strain gauge and displacement sensor instrumentation.

Component	*Normal Strain*	*Shear Strain*	*Displ. points*	*Reaction Forces*	*Loads**	*Load Cases*
Wing L/H	44	17	8	6	4	27
Fuselage	45	28	28	12	4	35
Horiz. stabilizer L/H	32	8	8	-	4	24
Aileron L/H	7	4	10	-	2	20
Flap L/H	7	5	10	-	2	22
Rudder	5	6	8	-	1	12
Elevator L/H	6	6	10	-	2	14
Elevator R/H	5	5	10	-	2	14
Main landing gear leg L/H	12	-	7	-	1	11
Engine mount	20	-	9	-	2	22

**: Max no. of applied loads per load case*

DIC measurements

DIC is a non-contact optical technique to determine full-field deformation data [7]. The method is based on tracking the local motion at the studied surface, which is discretized into small areas called generally as subsets. A random pattern with high contrast is generally applied to the tested surfaces by paints. In this case, the random speckle pattern was generated by stamping the test surface with water-diluted black acrylic matt paint using a sponge. Depending on the recording distance, and thus the desired size of the speckles, different sponges were used.

3-D DIC measurements were carried out with a commercial setup from LaVision consisting of two 5 MPix CCD cameras, two pulsed LED-lights and a device control unit. An example of the test setup is presented in Figure 5. The targeted length of the field of view in the recorded images ranged between 0.4 m…1.8 m. Excluding the tests with the fuselage, the tested components were aligned horizontally in the testing jig. Thus, the normal of the studied surface pointed upwards and the cameras were positioned above the component. The images were acquired with objectives having a focal length of 24 mm, which resulted that the distance of the cameras to the studied component ranged approximately between 1.5 m and 6 m depending on the size of the studied area. The different imaging setups resulted pixel-to-mm scaling factor to range between 1.5 pix/mm to 5.1 pix/mm.

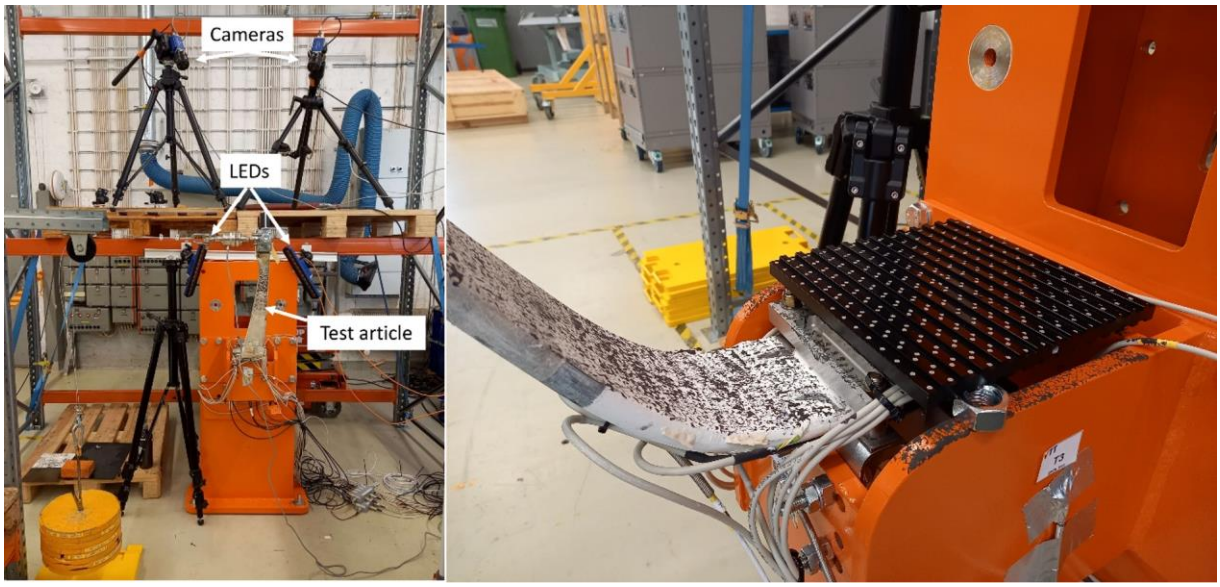

Figure 5: Left: 3-D DIC test setup. Right: the calibration plate on top of the test article with the DIC speckle pattern.

Before testing, the calibration of the DIC setup had to be performed to link the pixel information of the recorded images to the 3-D world position coordinates of the tested component. This was performed with a 3-D calibration plate (Figure 5) of which 5 to 10 images were acquired in different positions covering the full 3-D space of the studied surface. The actual calibration was performed with the used DIC software (Davis 10.2.0 by LaVision). After calibration, ten images were acquired from the unloaded component which were used as the reference images in the DIC analysis. During a load case, ten images were taken from each load step.

The recorded images were processed into displacement and strain field data with the above-mentioned software. The subset and step sizes in the analysis were altered with the tested components to optimize the spatial resolution and the measurement noise. Typical values for the subset and step sizes were 25 and 8 pixels, respectively. The values resulted the spatial resolution, or the distance of two adjacent displacement measurement points, to range from 2.6 mm to 5.4 mm for the smallest and largest components, respectively. Ten separate measurements were determined from each loading step and their resulting averages were used as the representative values in the later analysis.

Comparison of strain gauge and displacement sensor results versus DIC results: Main landing gear leg

The main landing gear leg is made of steel, and it was installed in the test jig's leg support box using its own attachment brackets upside down to enable loading by weights and a turnbuckle. A wheel axle dummy was attached to the leg to provide a representative location as loading point and about 50% of the loads calculated according to FAR23 were applied in multiple steps. The load case selected for this comparison was FAR23.479 (Level landing - MLG only) in which the maximum test load was slightly below 8 kN.

The leg was instrumented with strain gauges on upper and lower surfaces close to the inner attachment bracket and on both sides (inner/outer) of the outer bracket. Seven laser displacement sensors were attached to the leg's support box in the jig and installed to measure the deflections (with ref. to the support box) of the leg between the attachment brackets. The DIC cameras were set on a separate stand and the measurement area was selected to cover a moderate sized area with length of ≈400 mm from the inner end of the leg. Also, the top edges of the support box side walls were included to the DIC measurements for estimating the deflections of the jig and the support box (line A, figure 6). When comparing DIC results against results from strain gauges and displacement sensors, data from strain channels S41, S43 and S45 and displacement channels SM1, SM3 and SM5 were used (figure 6). Strain data from DIC was extracted next to the strain gauge and its protective mass. Displacement values from DIC were taken from the line B. Displacement data acquired by DIC from the line A was used to create

corrections for DIC displacement values by taking the deflection of the support box into account when determining the leg's true deformation.

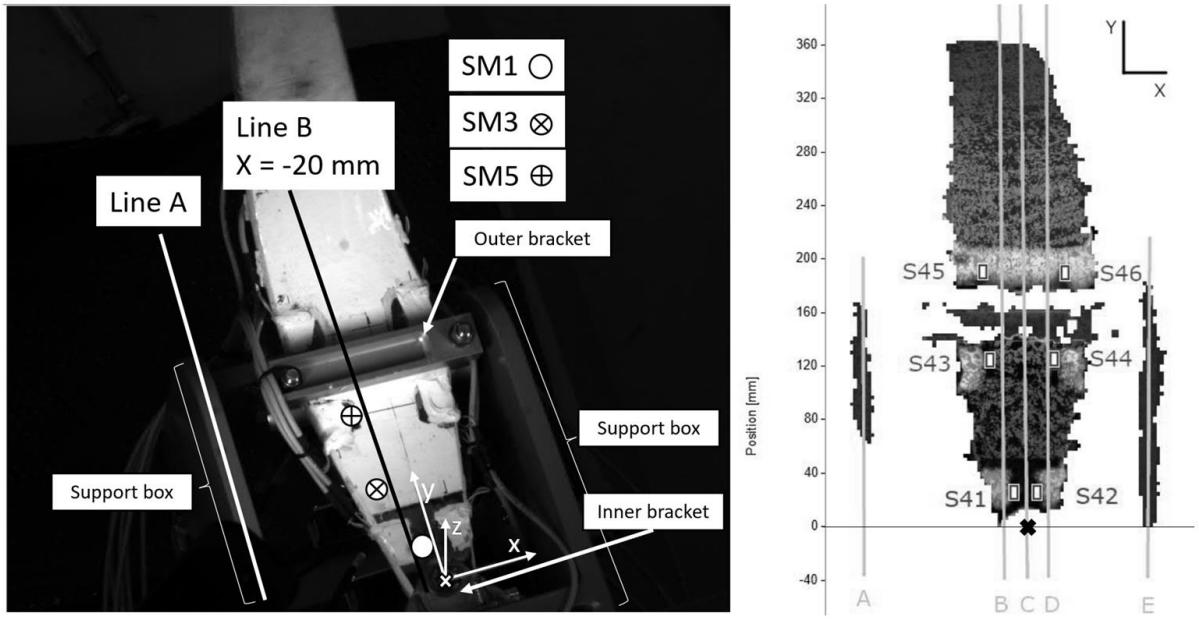

Figure 6: Lines A and B for DIC data extraction and positions of used displacement (SM1-3) and strain (S41, S43 and S45) channels

At the maximum test load, the leg tip displacements were 130 mm up and 114 mm outboard (directions ref. to aircraft; measured manually), the maximum of laser sensor displacements showed 1.362 mm (SM3) and the strain gauges about ±4000 μm/m (S45) positive values being on the side visible to DIC. The DIC strain estimates were in good agreement with the strain gauges (see figure 7). The maximum DIC vertical displacements were ≈0.2-0.3 mm smaller compared to those acquired by laser sensors. However, when the DIC results are compensated for jig displacements by subtracting the z-displacement values calculated by the linear fit shown in the figure 7, the displacement results are in good agreement at all three studied points. Both result sets, strains, and displacements, showed fairly linear response the only major exception being the DIC results near the inner bracket (S41). This encountered slight nonlinearity is presumably the net result of the decreased contrast in the DIC images due to inferior local surface pattern and lighting conditions caused by the adjacent attachment bracket, and the thin layer of the strain gauge's protective mass existing on the leg's surface partly at the DIC data collecting area.

The detailed reports of the ground tests for the L/H main landing gear leg can be found in references [8, 9].

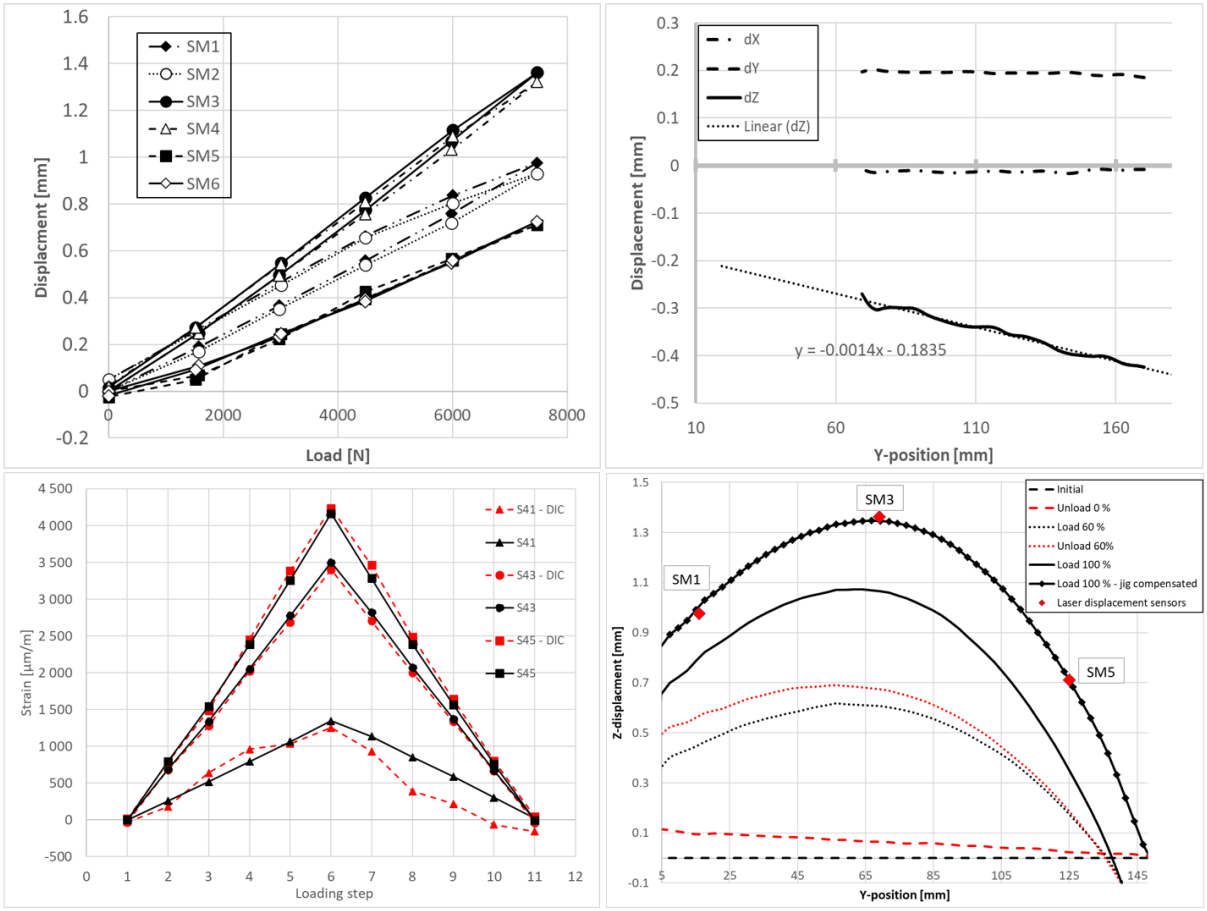

Figure 7: Up left: Laser displacement sensor response showing linear response. Up right: DIC results from the line A showing the deformation of the jig. Down left: Measured strains from strain gauges and DIC showing linear response and correlation between results. Down right: Displacements from DIC at the line B and from laser sensors showing the correlation between laser sensor results and jig deformation compensated DIC results.

Comparison of displacement sensor results versus DIC results: L/H wing

Because the applied loads for the wing were heavily limited due to the loading setup, it was clear in advance that the test loads will not produce strains of usable magnitude for the used DIC setup. Thus, the displacements at wing root area were chosen as the main target for DIC. The DIC measurement area was selected to cover the whole wing chord and to reach the inner collar location ending up to a quite wide area of about 1.4 m x 1.6 m.

The ground test instrumentation included numerous additional ground test strain gauges on upper and lower surfaces of the wing and wing spars. Three laser displacement sensors were attached to the jig's wing root support beam to measure wing lower skin deflections (with ref. to the support beam) below the wing root shear pins and the wing main spar. Five more sensors were installed on supports resting on the floor to measure wing lower skin deflections near wing leading and trailing edges along the span and at wing tip under the main spar.

During the tests the maximum displacements shown by the laser sensors were 46 mm at the wing tip and 10 mm on the DIC measurement area, and the maximum strains shown by the strain gauges were usually below 280 µm/m, but about 440 µm/m for one gauge. For this comparison, the focus was set on a load case where the wing was bended downwards with a total load of around 1.6 kN. This load case yielded maximum displacements around 20 mm at the wing tip and 4.5 mm at the DIC measurement area. Largest measured strains were of magnitude 200 µm/m from few channels. The displacement

sensors in the area visible to DIC are SM71-75 (figure 8). The DIC data was extracted from spanwise lines X1 and X3 and from chordwise line Y1, which run close to the laser sensor locations.

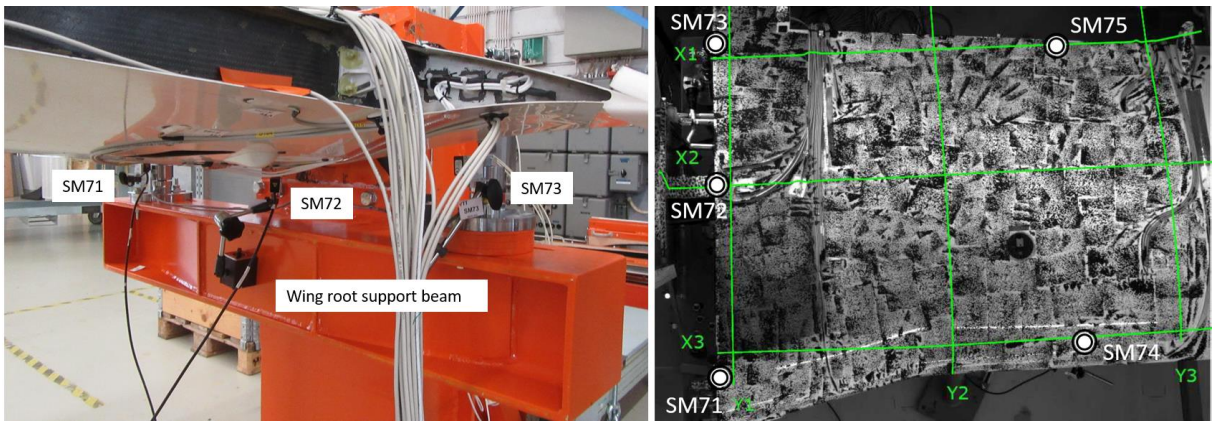

Figure 8: DIC measurement area for the wing root and the lines selected for reporting the DIC displacement results. Also, approximate locations of the five laser displacement sensors (SM71-75) used in the area (below the wing) are shown in the figure.

The displacement results with laser sensors and DIC for the selected load case are shown and compared in figure 9. Similar to the results from the main landing gear leg, the response of the structure is fairly linear as shown in the upper left picture of figure 9. As shown in the upper right and lower left pictures of figure 9, the displacement results between DIC and laser sensors are in good agreement. This data is uncompensated for jig bending since both the DIC cameras and the sensors SM74 and SM75 are mounted separately of the test jig and therefore share the same reference system. The lower right picture of figure 9 shows that the results from DIC and sensors SM71-73 did not correlate very well, although the displacement levels are very small. However, the shape of the displacement field along line the Y1 correlates between DIC and laser sensors i.e., the magnitude of error is approximately constant. Therefore, the slight difference in the results is presumably due to the jig deformations since sensors SM71-73 are mounted on the wing root support beam of the test jig. Also, the location of sensors SM71-73 differs around 30 mm from the line Y1, sensors being closer to the wing root rib which contributes to the resulting difference. The compensation for jig bending and possible other contributing factors has not been done, since the difference is small and the valuable information in the lower right picture of figure 9 is the shape of the chordwise deformation field.

The detailed reports of the ground tests for the L/H wing can be found in references [10, 11].

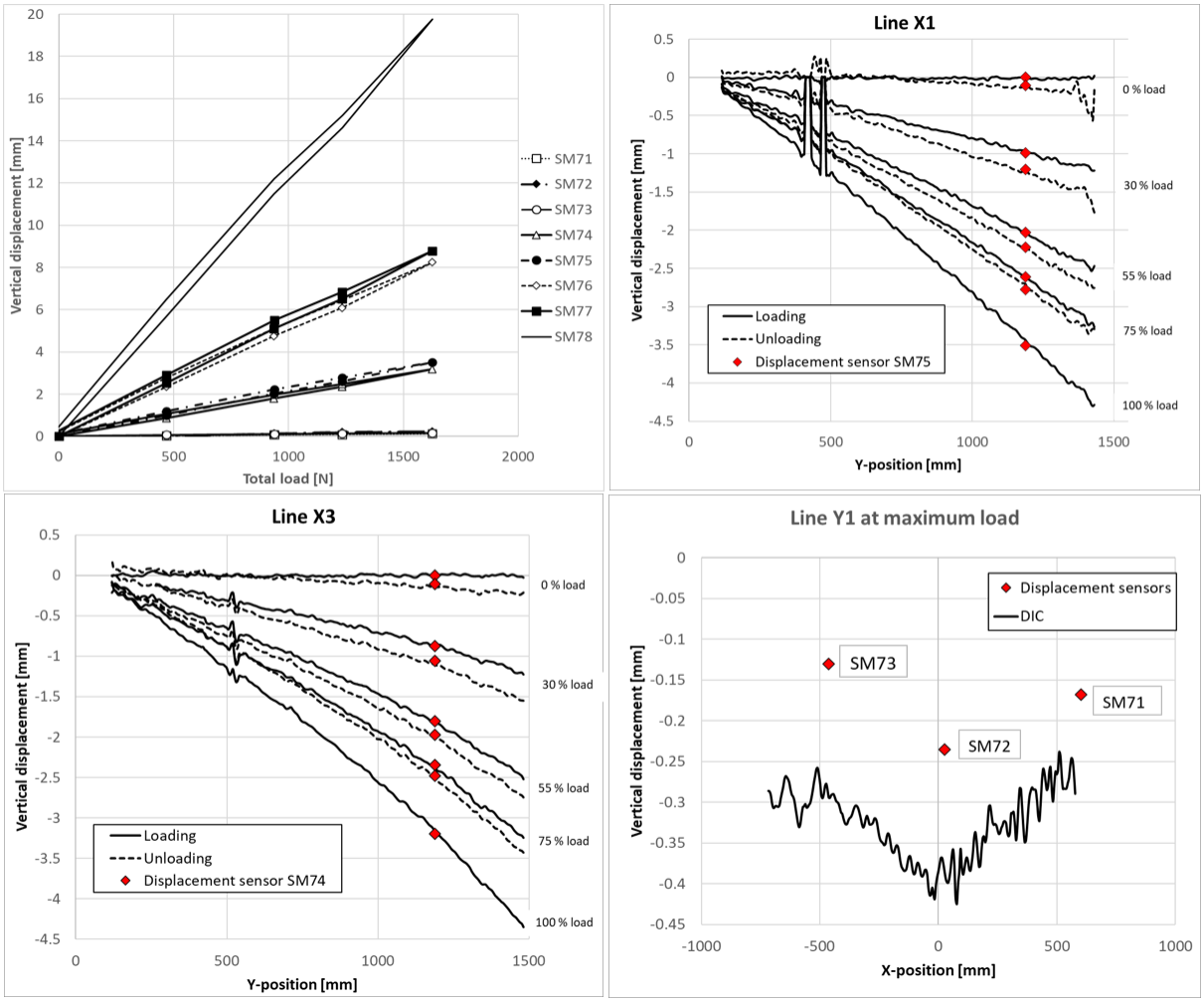

Figure 9: Up left: All laser displacement sensor results per load step showing the linearity of the results. Up right: Displacement results from line X1 and sensor SM75. Down left: Displacement results from line X3 and sensor SM74. Down right: Displacement results from line Y1 and sensors SM71-73.

SUMMARY

This paper presented the research performed on the two subprojects of the national MRO capability program: The flight and ground tests. Test programs, test setups, used instrumentations and, due to the vast amount of data, partial test results were presented. The flight test program covered the entire flight envelope and included FINAF training syllabi maneuvers. The measured strains during flight and calculated global loads were of expected magnitude. Flight test results have already been utilized when designing repairs and modifications to the hinge bracket attachment. The outcome of the ground tests was equally successful. The responses of the structures were linear and therefore the results are useful when validating the FE-models in the future. Also, the DIC measurement technique showed promising correlation when the results were compared to the measurement techniques of strain gauges and laser displacement sensors.

The next steps in the MRO program are material tests and construction of the component FE-models. Material values of the composites of the aircraft together with the flight test data will create a solid base to estimate the fail-safe principles included in the design and to make engineering decisions regarding damage repairs and modifications. This base is further solidified with the FE-models which will be validated using the ground tests results. This increases the reliability of the FE-models which in turn increases the national understanding of the characteristics of the structure of the aircraft. The flight test

data including the FINAF training syllabi maneuvers will also permit the creation of a FINAF baseline operating spectrum for different components in the future.

REFERENCES

[1] Viitanen, T., & Siljander, A. (Eds.) (2019). *A Review of Aeronautical Fatigue Investigations in Finland April 2017 - March 2019*. VTT Technical Research Centre of Finland. ICAF National Review - Finland No. VTT-CR-00352-19

[2] Viitanen, T., & Siljander, A. (2021). *A Review of Aeronautical Fatigue Investigations in Finland April 2019 - April 2021*. VTT Technical Research Centre of Finland. ICAF National Review - Finland No. VTT-CR-00448-21

[3] Ripatti, A. *Loads required by FAR-23 for Grob G115E*. Patria Aviation Oy. Technical report No. GO-S-0009 (in Finnish, classified, not yet published).

[4] Hukkanen, T. (2021). *Grob structural research: Flight test report*. Patria Aviation Oy Technical report No. GO-S-0025 (in Finnish, classified).

[5] Liukkonen, S. (2021). *Grob G 115E Mini-OLM flight test measurements.* Technical Research Centre of Finland Ltd. Report No. VTT-R-00440-19 (in Finnish, classified).

[6] Laatikainen, Y., Hukkanen, T., Vuori, M. (2020). *GO-mini-OLM flight test preparation report.* Patria Aviation Oy. Technical report No. GO-S-0011 (in Finnish, classified).

[7] Jones, M.A., Iadicola. E.M.C. (2018), *A Good Practices Guide for Digital Image Correlation,* International Digital Image Correlation Society, DOI: 10.32720/idics/gpg.ed1

[8] Orell, O., Jokinen, J., Kanerva, M. (2022). *K1 - DIC-analysis of main landing gear leg*. Tampere University. Technical report (in Finnish, classified).

[9] Liukkonen, S. (2022). *Grob Ground Tests K1 – L/H Main Landing Gear*. Technical Research Centre of Finland Ltd. Report No. VTT-R-00513-22 (in Finnish, classified).

[10] Orell, O., Jokinen, J., Kanerva, M. (2022). *K9 - DIC-analysis of L/H wing*. Tampere University. Technical report (in Finnish, classified).

[11] Liukkonen, S. (2022). *Grob Ground Tests K9 – L/H Wing.* Technical Research Centre of Finland Ltd. Report No. VTT-R-00797-22 (in Finnish, classified).